DYNA
ISSN: 0012-7353
ISSN: 2346-2183
Universidad Nacional de Colombia

Effects of strain on $L\#_{0.67-x}Pr_xC\#_{0.33}Mn0_3$, $L\#Mn_{1-X}C0_x0_3$ and $L\#Mn_{1-x}Ni_x0_3$ magnetite samples

Olarte-Torres, Javier Alberto; Cifuentes-Arcila, María Cristina; Suárez-Moreno, Harvey Andrés

Effects of strain on $L\#_{0.67-x}Pr_xC\#_{0.33}Mn0_3$, $L\#Mn_{1-X}C0_x0_3$ and $L\#Mn_{1-x}Ni_x0_3$ magnetite samples
DYNA, vol. 86, no. 211, 2019
Universidad Nacional de Colombia
Available in: http://www.redalyc.org/articulo.oa?id=49663345032
DOI: 10.15446/dyna.v86n211.78081

Artículos

Effects of strain on $La_{0.67-x}Pr_xCa_{0.33}MnO_3$, $LaMn_{1-X}CO_xO_3$ and $LaMn_{1-x}Ni_xO_3$ magnetite samples

Efectos de las tensiones en muestras de magnetitas de $La_{0.67-x}Pr_xCa_{0.33}MnO_3$, $LaMn_{1-X}CO_xO_3$, and $LaMn_{1-x}Ni_xO_3$

Javier Alberto Olarte-Torres [a] jaolartet@udistrital.edu.co
Universidad Distrital FJC, Colombia
María Cristina Cifuentes-Arcila [b]
mcifuentes@pedagogica.edu.co
Universidad Pedagógica Nacional, Colombia
Harvey Andrés Suárez-Moreno [b]
hasuarezm@pedagogica.edu.co
Universidad Pedagógica Nacional, Colombia

DYNA, vol. 86, no. 211, 2019

Universidad Nacional de Colombia

Received: 25 February 2019
Revised document received: 20 August 2019
Accepted: 14 November 2019

DOI: 10.15446/dyna.v86n211.78081

Abstract: This paper presents the results obtained from the synthesis and morphological characterization of different magnetite samples: $La_{0.67-x}Pr_xCa_{0.33}MnO_3$ at $0.13 \leq x \leq 0.67$ produced by a solid-state reaction mechanism and $LaMn_{1-x}Ni_xO_3$ at $0.0 \leq x \leq 0.5$ produced by the sol-gel method. These samples were characterized using X-ray diffraction spectroscopy and by measuring electric resistivity and magnetic susceptibility which were carried out as a function of temperature. Notably, the effects of strain and compressive strength on the lattices of magnetite samples were highly dependent on the concentration of *Pr*, *Co* and *Ni*. Moreover, the transition temperatures of metal-insulator and ferromagnetic-paramagnetic phases also largely depend on these strength effects, *e.g.*, at higher concentrations of *Pr*, effects of increased strain strength were observed, relocating the shifts of ferromagnetic-paramagnetic transitions to lower temperatures. On the other hand, effects of increased compressive strength were observed at higher concentrations of *Ni* and *Co*, relocating the shifts of ferromagnetic-paramagnetic and metal-insulator transitions to higher temperatures.

Keywords: magnetite, strain strength, Curie temperature, transition temperature.

Resumen: Se reporta la síntesis y la caracterización de manganitas de $La_{0.67-x}Pr_xCa_{0.33}MnO_3$ con$0.13 \leq x \leq 0.67$, obtenidas por reacción de estado sólido, y de $LaMn_{1-x}Ni_xO_3$, con $0.0 \leq x \leq 0.5$, obtenidas por el método sol-gel. Las manganitas se caracterizaron a través de medidas difracción de rayos X, resistividad eléctrica y susceptibilidad magnética en función de la temperatura. Se concluyó que los esfuerzos de tensión y compresión en la red dependen fuertemente del contenido de, *Pr*, *Co* y *Ni* en las muestras, y que las temperaturas de transición de las fases metal-aislante y ferromagnética-paramagnética depende fuertemente dichos esfuerzos: a mayor contenido de *Pr* se produjo mayores esfuerzos de tensión que desplazaron el corrimiento de la transición ferromagnética-paramagnética a temperaturas más bajas, mientras que a mayor contenido de *Ni* y *Co* se produjo mayores esfuerzos de comprensión que desplazaron el corrimiento de las transiciones metal-aislante y ferromagnética-paramagnética a temperaturas más altas.

Palabras clave: manganitas, esfuerzos de tensión, esfuerzos de compresión, temperatura de Curie, temperatura de transición.

1. Introduction

The discovery of colossal magnetoresistance (CMR) in magnetite materials has motivated the study of their remarkable physical properties. For instance, the role that doped holes play in the CMR of magnetite materials is well known. Specifically, for Manganese Oxide and Manganese doped with Cobalt/Nickel, the CMR effect has been explained by means of a double-exchange mechanism for samples. Nonetheless, there are different points of view as to the formal charge of either cobalt or nickel and the interaction #o(3#)−# (2#)−#n(3#). Goodenough [1] has suggested that the charge distribution for the compound distribution in and samples should be trivalent either of cobalt or nickel with a low spin state (for Co^{3+} and for Ni^{3+}) and the resultant ferromagnetic interactions (Ni^{3+}, Co^{3+}) - 0^{2} -Mn^{3+} allow a spontaneous magnetization to occur in such compounds. Toulemonde [2] employed X-ray absorption spectroscopy (XAS) at high energies and noticed the formal charge from dopant elements are mostly seen in Ni^{2+} and Co^{2+}, which aligns with the results obtained by Blassel [3] for compounds of , suggesting that the ion combinations of Co^{2+} (Ni^{2+}) and Mn^{4+} should be more stable than trivalent ions. Consequently, these authors established that the exhibited ferromagnetic effects of the samples studied are governed by strong interactions between ions of (Ni^{2+}, Co^{2+}) - 0^{2} -Mn^{4+}. In contrast, it is well known that the matrix compound of $L\alpha Mn0_3$ is antiferromagnetic and it is relatively easy to induce the ferromagnetic effect using cationic substitution [4]. A notable example is the substitution of alkaline earth metal ions such as $C\alpha^{2+}$ or Sr^{2+} at the A-site of $L\alpha Mn0_3$, which carries out paramagnetic-ferromagnetic transitions bounded by magnetoresistance effects. Furthermore, from a theoretical perspective, the substitutions at the manganese site are noteworthy owing to the important role that the lattice of manganese-oxygen plays in terms of the physical behavior of such materials. The cationic substitutions could produce certain changes in the physical properties of both conductive ferromagnetic manganites and the insulator compound of ordered charge. The orbital-ordered ferromagnetic state of $L\alpha Mn0_3$, is easily destroyed, which causes ferromagnetism, but this ferromagnetic behavior can take place by means of several mechanisms, depending on the cation and level substitution. The physical properties can be derived from a complex interaction between the exchange interactions, the orbital-ordered state, and Jahn-Teller distortion (JT) [5-13].

To give another example, an increase of either the length or angle of an *Mn - 0 - Mn* bound tends to trace the charge carrier, and, furthermore, reduces the double exchange interaction, modifying the Curie temperature (T_c.) of the magnetite [14].

In terms of biaxial compression, the stress components σ_{zz} , σ_{xy} , and σ_{yz} are equal to zero. Given by the formula $\varepsilon_{xx} < \varepsilon_{zz} < 0$ (compressive

strain), and where (is Poisson's ratio, the strain component along the normal of the thin film can be written as

$$\varepsilon_{zz} = \frac{2v}{1-v}\varepsilon_{xx} \qquad (1)$$

As an initial approach, assuming that the volume will be conserved, it can be concluded that $\varepsilon_{xx} = -2\varepsilon_{xx}$ when $V = 0.5$. As the majority of materials have values for V that are between 0.3 and 0.5, their biaxial distortion can be given by the equation $\varepsilon_{bi} = ¼ (2\varepsilon_{zz} - \varepsilon_{xx}\ \varepsilon_{yy})$. that translates as tensile strengths of $\varepsilon_{bi} < 0$ and compressive strains of $\varepsilon_{bi} > 0$.

In this paper, we analyze the effects of strain on the magnetite samples and at different doping levels.

2. The effects of strain on magnetite

2.1. The effects of strain on Lα 0.67-x Pr x Cα 0.33 Mn0 3 magnetite samples

The magnetite samples were produced using a solid-state reaction method in which high purity $L\alpha_2\#_3$, Cα0, $\#n_2\#_3$, and $\#r_2\#_3$ dusts were mixed. The resultant materials were mixed and heated at 800 °C for 16 hours, then pulverized and heated again at 850 °C for 32 hours. Subsequently, the obtained material was mixed again and heated at 950 °C for 64 hours. Finally, the samples were encapsulated and heated at 1200°C for 8 hours. These processes were performed at standard conditions of pressure under which different heat treatments and exposition times contributed to the production of high crystalline quality in the samples.

As depicted in Fig. 1, the crystalline structure of the sample was observed and characterized by X-ray spectroscopy, specifically the X-ray Diffraction Technique (XRD), whose data was processed with X'Pert Plus software. Secondary phases were not observed in the collected spectrum using XRD. In this respect, Table 1 shows data referring to the variation of the lattice parameters at different concentrations of Praseodymium Pr. When Pr concentration is increased, the lattice constant parameters gradually decrease. This result could be attributed to the different ionic ratios of Lanthanum and Praseodymium of around 1.15 Å and 1.09 Å respectively. The presence of Pr causes a shift in the peak signal detection that is well-observed at its peak (202) and shifts from 2(= 32.781 and 32.700 (see x-axis in Fig. 1) and shows a full width at half maximum (FWHM) of less than 0.5117, indicating high crystalline quality for bulk samples.

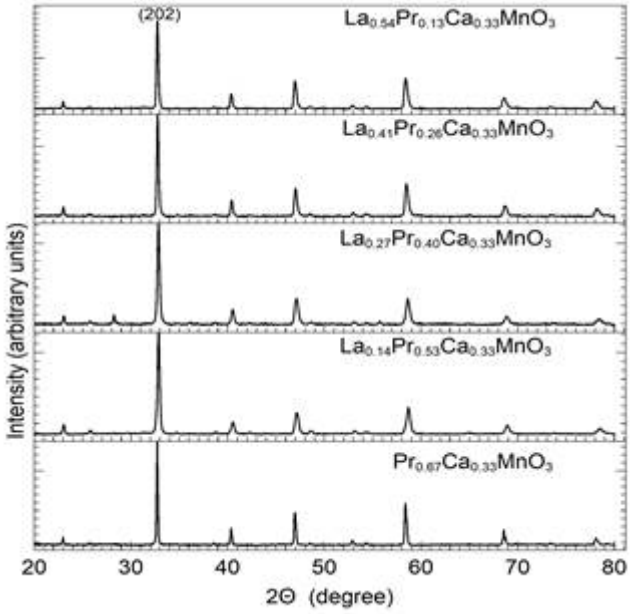

Figure 1
The XRD patterns of the $L\alpha_{0.67-x}Pr_x$ $C\alpha_{0.33}Mn0_3$, samples with $0.13 \leq x \leq 0.67$.
Source: The Authors.

Table 1
Lattice constants and unit cell volume of $L\alpha_{0.67-x}Pr_x$ $C\alpha_{0.33}Mn0_3$ samples with $0.13 \leq x \leq 0.67$.

Pr concentration x	Lattice constant a (A)	Lattice constant b (A)	Lattice constant c (A)	Unit cell volume (A^3)
0.13	5.4568	5.4625	7.6954	229.38
0.26	5.4451	5.4490	7.6855	228.03
0.40	5.4411	5.4398	7.6759	227.19
0.53	5.4334	5.4387	7.6699	226.65
0.67	5.4239	5.4380	7.6629	226.01

Source: The Authors.

Another important result is depicted in Fig. 2 and shows the behavior of the lattice constant and the unit cell volume which decreases by around 3% due to the smaller ion size of the Praseodymium. Notably, all samples exhibited an orthorhombic structure in pbmn (62) space group.

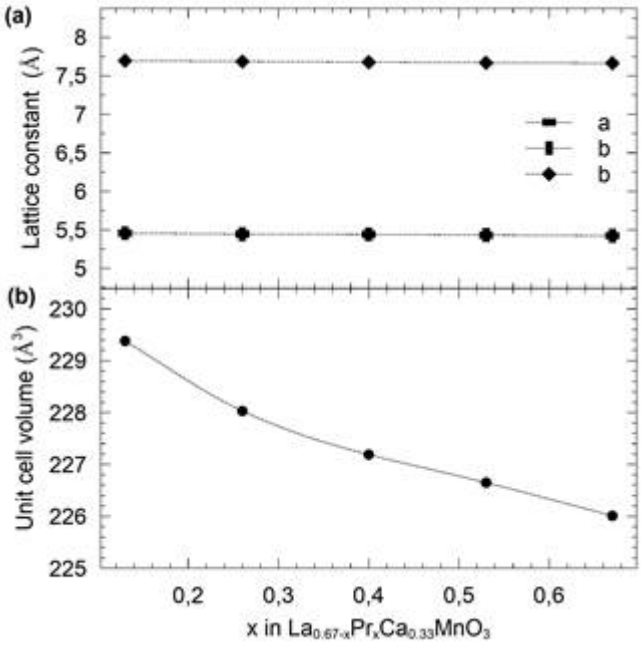

Figure 2

Lattice constants (a) and unit cell volume (b) variation as a function of Pr concentration in $L\alpha_{0.67-x}Pr_x\ C\alpha_{0.33}Mn0_3$ samples. Dashed lines are visual guides.

The substitutions of Pr with an ionic ratio less than that of Lα produced a decrease in Curie temperature T_c as a function of the concentration of Praseodymium (see Table 2). Such experimental results are mirrored in other related research [15,16].

Table 2

Biaxial strain, Curie temperature, transition temperature, activation energy and electrical resistivity for $L\alpha_{0.67-x}Pr_x\ C\alpha_{0.33}Mn0_3$ samples with $0.13 \leq x \leq 0.67$.

	***Pr* concentration x**			
	0.13	**0.26**	**0.40**	**0.67**
Electrical resistivity (Ω/m)	1.43	0.25	0.12	0.05
Biaxial strain (%)	-0.2322	-0.3283	-0.4216	-0.57795
Curie temperature (K)	244.55	140.88	122.90	117.92
Transition temperature (K)	211.69	145.84	115.87	141.82
Activation energy ($x10^8$ meV) (ASPH)	138.45	152.24	170.89	219.16

Source: The Authors.

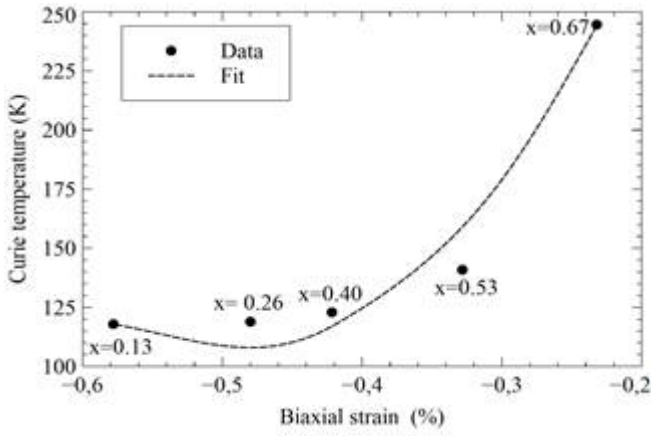

Figure 3
Evaluated biaxial strain versus Curie temperature for different compositions of $L\alpha_{0.67-x}Pr_x\ C\alpha_{0.33}Mn0_3$ samples with $0.13 \leq x \leq 0.67$. Second degree polynomial (dashed line) fitting the defined evaluated setpoints (dots).
Source: The Authors.

The above result can be understood as follows: on one hand, the substitutions of Lα ions for a smaller ones, like those of Pr reduce the average ionic ratio $<r_A>$ which causes a decrease in the electronic coupling matrix element b which describes the electrons hopping among the different sites of Mn. The change in # emerges as a consequence of the structural changes that modify Mn - 0 - Mn either through angle or length variations of such bound states [17].

On the other hand, the decrease of the average ratio of A-sites $<r_A>$ is related to the decrease in the θ angle of the Mn - 0 - Mn bound due to a rotational action of the octahedrons that reduces the distance between the A-sites. When # is decreased, a decrease in b and T_c are also observed [17-19].

To clarify the role that the biaxial strain plays, different studies have been performed using ultrathin films and hetero-structures [16]. From these, it is expected that the effects produced by the strain test-induced by the substrate-are different in bulk samples, which influence the relationships between spin, charge, structure, and orbital degree of freedom.

In this context, our calculation of biaxial strain (ε_{bi}) produced by the substitution of Lα with Pr in the compound $L\alpha_{0.67-x}Pr_x\ C\alpha_{0.33}Mn0_3$ has been performed assuming, as an initial approach, that the volume of the unit cell is constant. The variations of volume from the unit cell are less than 3% in all cases and were determined by X-ray measurements.

In the case of the mentioned samples, the "tensile" strain effect ($\varepsilon_{bi} < 0$) increases with the concentration of Pr. Fig. 3 depicts the behavior of ε_{bi} vs. Curie temperature (T_c) and shows the increment in ε_{bi} that causes a decrease in T_c . An approximated quadratic relation is found in the experimental data (dashed line-fit).

Notably, T_c decreases when strain increases and it can therefore be assumed that the biaxial strain increases the Jahn-Teller splitting of the

e_g levels, which greatly contributes to the determination of the location of electrons. Such results were predicted by Millis and his collaborators [20-22].

The results of the transport mechanism are examined in the context of the data of resistivity obtained at different temperatures $T > T_c$. Thus, T_T stands for the temperature of the metal-insulator transition derived from the maximum derivative of dρ/dT. Remarkably, T_t is similar to T_c and decreases when the biaxial strain is increased. It has been suggested that the rate of temperatures $T > T_T$ has a strong effect on polarons [23], in terms of fitting experimental data from transport mechanisms, in which Adiabatic Small Polaron Hopping (ASPH) is considered, and is calculated as follows:

$$\rho = \rho_0 T exp\left(\frac{E_a}{K_B T}\right) \quad (2)$$

Similarly, Non-adiabatic Small Polaron Hopping (NASPH) is written as

$$\rho = \rho_0 T^{3/2} exp\left(\frac{E_a}{K_B T}\right) \quad (3)$$

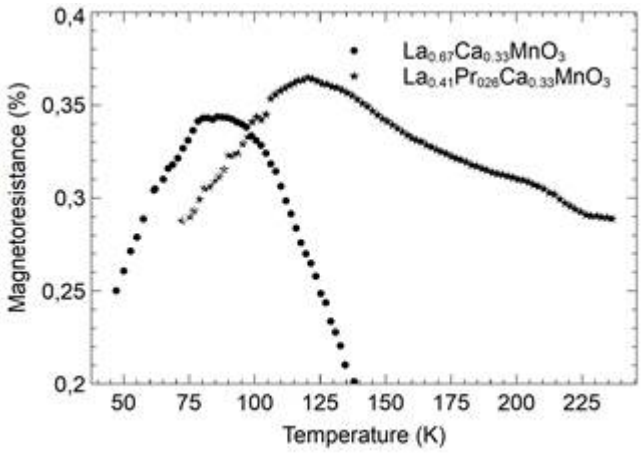

Figure 4
Magnetoresistance as a function of temperature for $L\alpha_{0.67-x}Pr_x$ $C\alpha_{0.33}Mn0_3$ and $L\alpha_{0.41}Pr_{0.26}$ $C\alpha_{0.33}Mn0_3$ samples.
Source: The Authors.

where $E\alpha$ stands for the activation energy and K_B the Boltzmann constant. A change of temperature rate is observed that is used for the fitting, which also depends on the value of the biaxial strain. In addition, the resistivity properties of the samples increase with the concentration of Pr, i.e., the increment of ε_{bi} . The activation energies derived from such fittings increase when the biaxial strain is high (see Table 2), which implies a Jahn-Teller-like increment of the lattice distortion in which an increment of $E\alpha$ would be caused, owing to a greater location of conductive electrons that increase the resistivity and reduce T_c .

In contrast, the samples at different rates of biaxial strain when measured for magnetoresistance #R=[#(#)−#(#)]/#(#) (see Fig. 4) exhibited an increase in MR with a remarkable decrease in T_c . A similar trend has been observed in multi-layers tested over different periods and with doped bulk samples, in which a decrement of the difference between the resistivity of the metallic and insulator regimes takes place as the temperature increases. The general observed trend of the MR obeys Eq. (4) [16], as follows,

$$MR \propto \frac{1}{T_t} exp\left(\frac{E_a}{K_B T_t}\right) \qquad (4)$$

2.2. The effects of strain on LαMn 1-x Co x 0 3 magnetite samples

The #α#n$_{1-\#}$##$_3$ (#=#o,#i) magnetite samples were analyzed by examining strain effects obtained from different substitutions of B-site with magnetite. To correlate the observed effects of the strain tests on the samples, an analysis of their electric and magnetic responses was performed. An analysis of the behavior of the #α#n$_{1-\#}$Co$_x$#$_3$ sample was performed first and an analysis of the #α#n$_{1-}$#Ni$_x$#$_3$ sample second.

The #α#n$_{1-\#}$(#o/#i)$_\#$#$_3$ samples were prepared using the sol-gel technique using a solution of lanthanum nitrate #α(##$_3$)$_3$ (0.1#),, manganese nitrite #n(##$_3$)$_2$ (0.1#), cobalt nitrite #o(##$_3$)$_2$ (0.1#), a stoichiometric ratio of nickel nitrate and citric acid #$_6$#$_8$#$_7$ (0.2#).. The obtained solution was jellified and heated to 100 °C and finally the obtained foam was heated at 600 °C for 4 hours.

Fig. 5 depicts the X-ray spectrum for different concentrations of cobalt where an orthorhombic structure with 62 space group pbmn can be observed. In such samples the chemical composition and morphology were determined by EDX and SEM, respectively. The inhomogeneity of the compositions is lower than 5%.

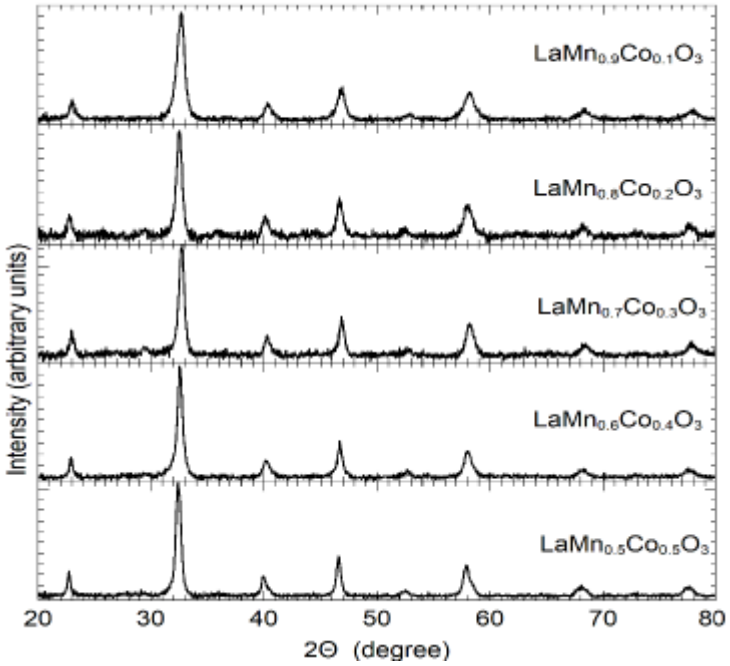

Figure 5
The XRD patterns of the #α#$n_{1-\#}Co_x\#_3$ samples with x = 0.0 to 0.5.
Source: The Authors.

Furthermore, several measurements of ac-susceptibility were taken using a Lake Shore 7000 susceptometer with a frequency of 20 Hz and a magnetic field strength of 800 A/m, with a range of temperatures between 80° K and 300° K.

The real and imaginary part of the susceptibility as a function of temperature for different concentrations of cobalt is shown in Figs. 7a and 7b. The paramagnetic-ferromagnetic/anti-ferromagnetic transition and Curie temperature (T_c) were obtained using the derivative of dX′/dT. Notably, the temperature T_c increases when the concentration of cobalt is increased, which can be related to the increased interaction of double-exchange. The observed peaks of susceptibility suggest that they can be understood as a spin-glass behavior related to competition between the ferromagnetic and anti-ferromagnetic interactions [24].

Table 3
Lattice constants and unit cell volume of the #α#$n_{1-\#}Co_x\#_3$ samples with x = 0.0 to 0.5.

Co concentration x	Lattice constant a (Å)	Lattice constant b (Å)	Lattice constant c (Å)	Unit cell volume ($Å^3$)
0.0	5.5320	5.7220	7.6990	243.7049
0.1	5.5272	5.6967	7.7508	244.0479
0.2	5.4316	5.4501	7.7470	229.3326
0.3	5.4254	5.4110	7.7457	227.3893
0.4	5.4231	5.4112	7.7418	227.1868
0.5	5.4126	5.4014	7.7069	225.3160

Source: The Authors.

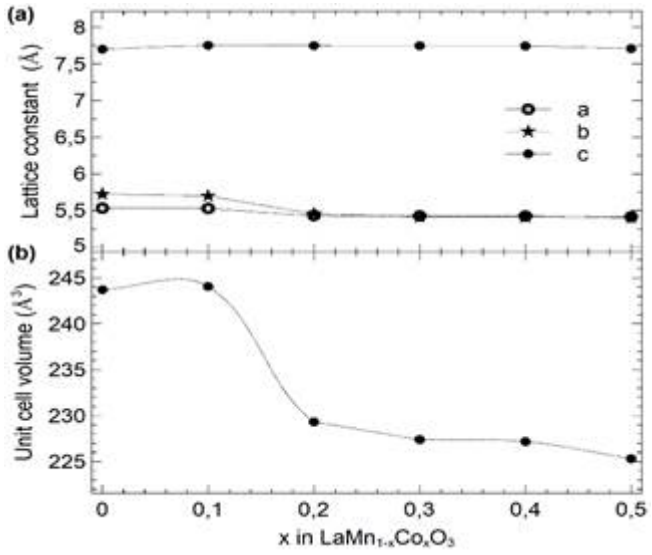

Figure 6
Lattice constants (a) and unit cell volume (b) variation as a function of Co concentration in #α#$n_{1-\#}Co_x\#_3$ samples. Dashed lines are visual guides.
Source: The Authors.

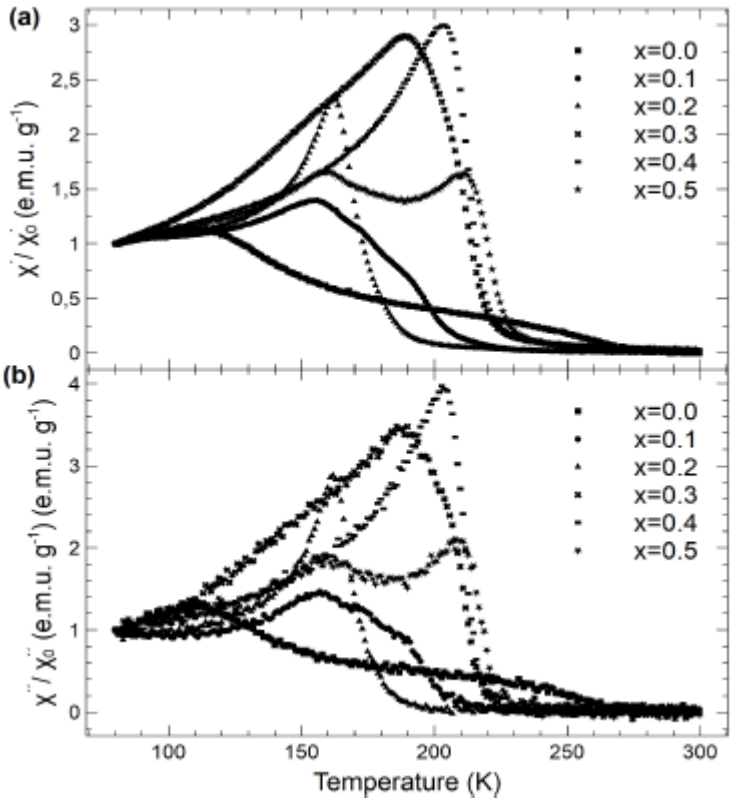

Figure 7
(a) Real (X/X_0) and (b) imaginary (X/X_0) component of the normalized ac-susceptibility as a function of temperature for different compositions of #α#$n_{1-\#}Co_x\#_3$ samples (x = 0.0 to 0.5).
Source: The Authors.

Fig. 8 shows the resistivity as a function of temperature for different concentrations of cobalt. A metal-insulator transition can be observed

where, at specific temperatures, the change in resistivity is abrupt and is denoted by T_t and determined by the maximum derivative of the resistivity vs. temperature (dρ/dT).

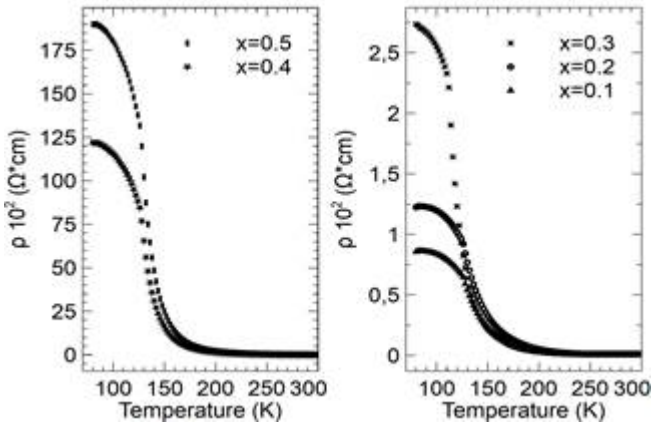

Figure 8
Resistivity (() as a function of temperature for different compositions of #α#$n_{1-\#}Co_x\#_3$ samples (x = 0.0 to 0.5).
Source: The Authors.

Table 4 lays out the assigned temperature for different levels of samples doped with cobalt. The increase in resistivity is closely related to the observed rise in activation energy and T_t , which can be attributed to an increase in electron hopping among the different sites of Mn. In this respect, T_t rises to higher temperatures when the concentration of cobalt increases, exhibiting a clear correlation between these occurances. However, the values of T_c and T_t do not coincide which can be attributed to the samples' magnetic inhomogeneity. This type of inhomogeneity is attributed to the multiple peaks that cross over into the imaginary part of the measured susceptibility.

Table 4
Biaxial strain, Curie temperature, transition temperature, activation energy and electrical resistivity for $LaMn_{1-x}Co_xO_3$ samples with x= 0.1, 0.2, 0.3, 0.4 and 0.5.

	Co concentration x				
	0.1	**0.2**	**0.3**	**0.4**	**0.5**
Electrical resistivity (Ω/m)	84.44	119.59	254.31	11456.56	17906.76
Biaxial strain (%)	0.376	0.4269	0.4548	0.4675	0.5046
Curie temperature (K)	163.87	-	211.77	212.73	220.75
Transition temperature (K)	102	-	122	125	250
Activation energy ($x10^8$ meV) (ASPH)	145.59	148.99	151.59	161.16	-

Source: The Authors.

In contrast, it is well known that there are remarkable differences in the magnetotransport properties for thin films and bulk materials which have been mainly been ascribed to biaxial strain induced by the substrate on the structure of the thin films owing to the differences in the lattice location (Lattice mismatch) between the film and substrate. In the case of magnetite samples with CMR, the coupling electron lattice plays a key role in understanding their electric and magnetic properties. The Jahn-Teller effect describes this coupling which is caused by biaxial distortions that allow the degeneracy levels of ## from the #n of a crystalline medium to be surpassed.

Table 4 indicates how the increase in the effects of strain produces a rise in the resistivity of the sample, i.e., the change in the constant lattice parameter can be explained by the small size of the cobalt ion in comparison to the $Mn^{3+/4+}$ ion. In addition, a double peak structure is observed in the susceptibility measurements which is produced by a high concentration of cobalt which, in turn, could be related to the strain effects and domain wall motion.

As depicted in Fig. 9, the increase in Co concentration in $LaMn_{1-x}Co_xO_3$ samples produced an increment of the biaxial strain ε_{bi} , which shifts Tc to higher temperatures. Such shifts can be explained by the substitution of Mn (B-sites) with Co ions, which are smaller (radius of Co^{3+} = 0.54 Å , radius of Ni^{3+} = 0.56 Å, radius of Mn^{3+} =0.58 Å).

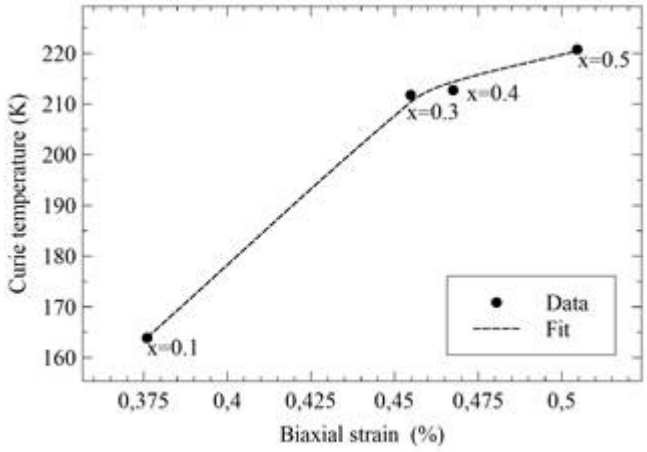

Figure 9

Evaluated biaxial strain versus Curie temperature for different compositions of $LaMn_{1-x}Co_xO_3$ samples (x = 0.0 to 0.5). Second degree polynomial (dashed line) fitting the defined evaluated setpoints (dots).

Source: The Authors.

2.3. Effects of strain on LaMn 1-x O 3 magnetite samples

The behavior of LaMn $_{1-x}$ Ni $_x$ O $_3$ samples at 0.1 < x < 0.5, in both magnetic and electric parts, was determined by taking magnetic susceptibility measurements (real and imaginary parts) and taking measurements of the resistivity as a function of temperature using the conventional four probe method.

All samples were characterized by taking measurements of X-ray diffraction (see Fig. 10), which shows an orthorhombic structure pbnm categorized within the 62 space group. The lattice constants a,b,c and the unit cell volume (V) were determined by Powder Cell software (see Table 5). As depicted in Fig 11, the lattice parameters decrease when exposed to the concentration of ##, which can be explained by the lower ionic radius of nickel (ionic radius of Ni = 0.60, ionic radius of Mn= 0.80)

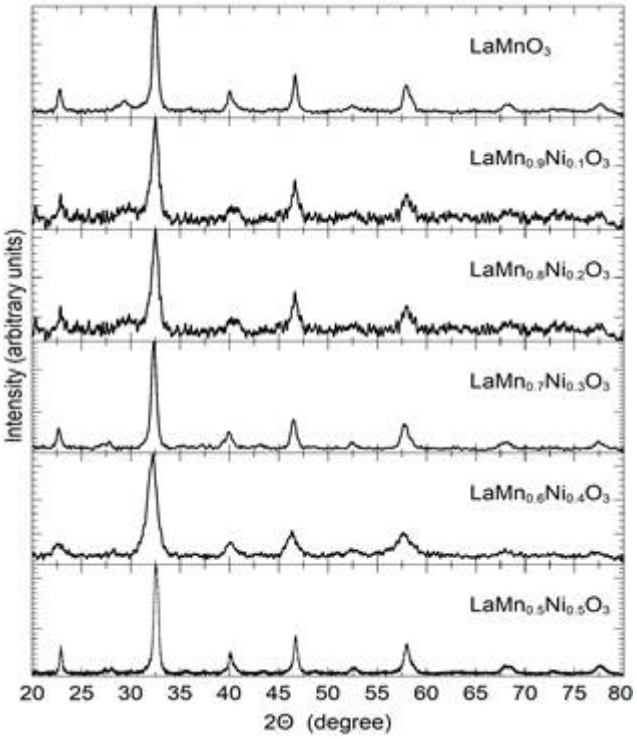

Figure 10
The XRD patterns of the $LaMn_{1-x}Ni_xO_3$ samples with x = 0.0 to 0.5.
Source: The Authors.

Table 5
Lattice constants and unit cell volume of the $LaMn_{1-x}Ni_xO_3$ samples with x = 0.0 to 0.5.

Ni concentration x	Lattice constant a (Å)	Lattice constant b (Å)	Lattice constant c (Å)	Unit cell volume ($Å^3$)
0.0	5.5320	5.7220	7.6990	243.705
0.1	5.5307	5.5822	7.7882	240.449
0.2	5.5290	5.5040	7.7918	237.117
0.3	5.5248	5.4710	7.7705	234.873
0.4	5.5199	5.4603	7.7536	233.696
0.5	5.5031	5.4540	7.7308	232.032

Source: The Authors.

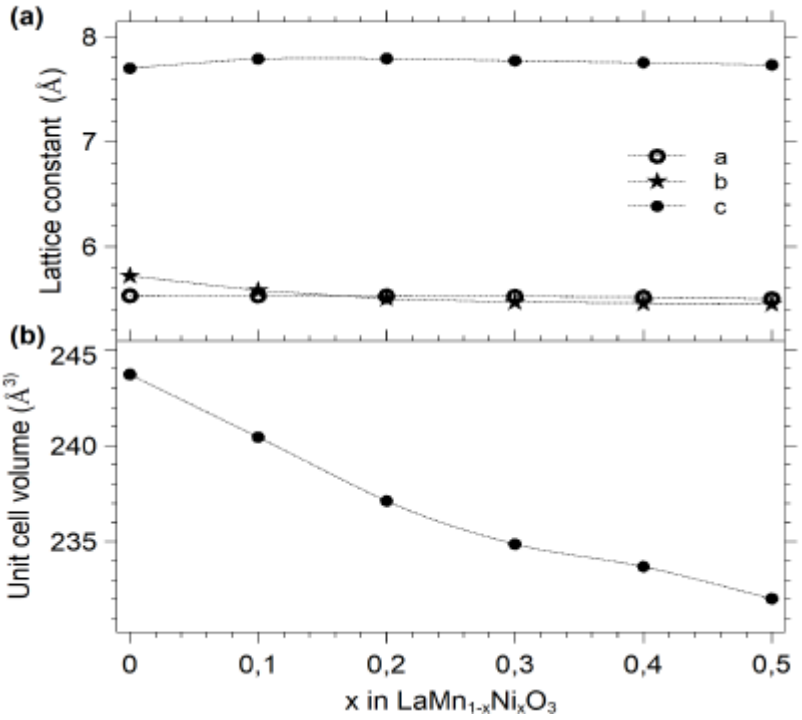

Figure 11

Lattice constants (a) and unit cell volume (b) variation as a function of Ni concentration in LaMn $_{1-x}$ Ni $_x$ O $_3$ samples. Dashed lines are visual guides.

Source: The Authors.

The spectrum from X-ray diffraction obtained exhibits a single-phase system; impure phases were not observed according to the equipment's indications.

Furthermore, the observed shifts are related to the different ion sizes of ##. Using EDX spectroscopy, the analysis of chemical composition shows variations from the stoichiometry < 5 % and the concentration of 0_2 was not substantially affected (variations of less than 2%) by the heat treatments to which the samples were subject.

As depicted in Fig. 12, the real (a) and imaginary (b) parts of normalized ac-susceptibility are shown (X/X $_{0,}$ and X/X $_0$ respectively) as a function of temperature for different concentrations of nickel.

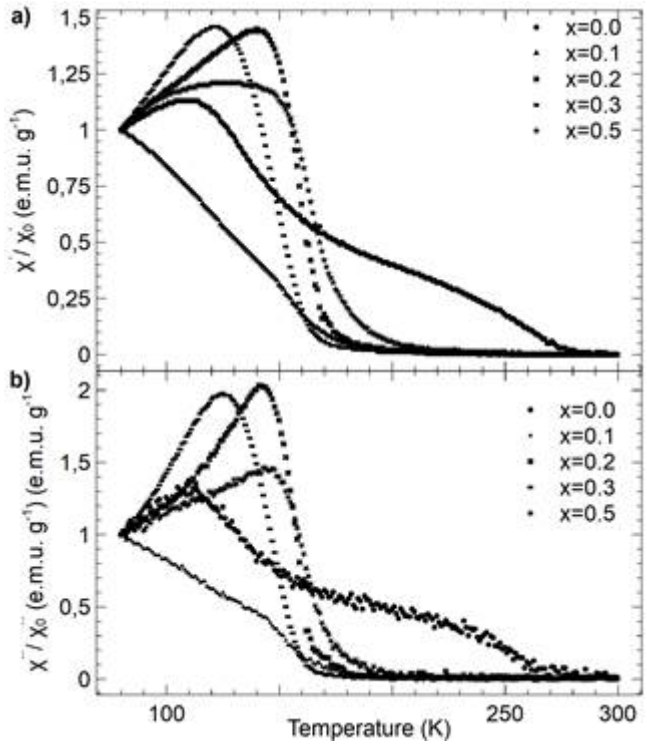

Figure 12
(a) Real (X/X_0) and (b) imaginary (X/X_0) component of the normalized ac-susceptibility as a function of temperature for different compositions of $LaMn_{1-x}Ni_xO_3$ samples (x = 0.0, 0.1,0.2,0.3 and 0.5).
Source: The Authors.

The Nickel-doped samples exhibit a remarkable behavior-which can be attributed to their spin-glass state-that can be observed as a peak in ac-susceptibility measurements. This behavior could be explained as the result of the competition between the antiferro and ferromagnetic regimes. Similar situations have been observed in different compounds [25]. It is well known that the orbital antiferromagnetic state of $\#\alpha Mn0_3$ is easily destroyed, resulting in a ferromagnetic state. Nevertheless, such ferromagnetic behavior could be the result of many other mechanisms that depend on the nature of substituted cations and substitutional levels [26].

The observed peaks that cross into the susceptibility measurements (X'/X') have been attributed to double-exchange interactions of $\#n^{3+}-\#_2{}^{2}--\#n^{4+}$,, which gradually vanish due to the interaction of an antiferromagnetic superexchange of the kind $\#n^{4+}-\#_2{}^{2}--\#n^{4+}$ and $\#i^{4+}-\#_2{}^{2}--\#i^{4+}$ [27].

Table 6 shows the transition temperatures of the insulated metal (T_t) and the magnetic transition (T_c) of the processes mentioned above. Although the transition temperature values do not explain any coincidence between the non-monotonic behavior and the concentration of Ni, all samples indicate a correlation between electric and magnetic phenomena. The general trend of different transition temperatures increases depending on the concentration of Ni.

Table 6

Biaxial strain, Curie temperature, transition temperature, activation energy and electrical resistivity for $LaMn_{1-x}Ni_xO_3$ samples with x = 0.0 to 0.5.

	Ni concentration x				
	0.1	0.2	0.3	0.4	0.5
Electrical resistivity (Ω/m)	1.65	18.69	46.38	87.91	31.50
Biaxial strain (%)	0.305	0.525	0.69	0.9	1.03
Curie temperature (K)	152.84	158.85	150.86	-	161.84
Transition temperature (K)	134.52	91.53	178.59	-	186.31
Activation energy (x10^8 meV) (ASPH)	126.39	142.08	157.87	-	-

Source: The Authors.

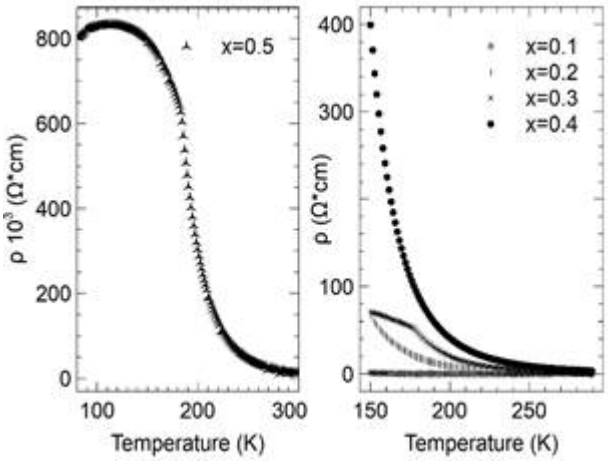

Figure 13

Resistivity (() as a function of temperature for different compositions of $LaMn_{1-x}Ni_xO_3$ samples (x = 0.1 to 0.5)

Source: The Authors.

The corresponding resistivity as a function of temperature for all nickel-doped samples is shown in Fig. 13. A metal-insulator transition was observed. The transition temperature T_t was determined by the maximum value of dR/dT vs. temperature. A significant increase in the resistivity as a function of the concentration of nickel was observed, and is depicted in the overlay of Fig. 10, which shows the resistivity of the sample that was a doped with 0.5.

The transition temperature (T_t) does not monotonically change when nickel is present, which correlates appropriately with the magnetic measurements (see Table 6). Nevertheless, T_c and T_t do not exhibit the same values, which is attributed to magnetic inhomogeneity. The inhomogeneity of the samples is characterized by multiple peaks in the imaginary part of the susceptibility [25].

The pseudo-perovskite RO_3 at the A-site is available and the applied pressure produces an increase in the rigid octahedron rotation RO_6. In the perovskite, the A-ion inhibits a possible collapse and the applied pressure decreases the rotation using the decrease in ionic radius mismatch which shows a denser packing of the 0_2 ion surrounding the ion at the A-site. Several papers that have studied the effects of pressure on $PrNi0_3$ samples and the results of crystallography of neutrons have confirmed that the octahedron $Ni0_6$ rotates less when pressure is applied; θ tends to 180° and the Ni- 0 bond is compressed.

In contrast, the measurements of resistivity as a function of temperature (see Fig. 13) are the outcome of the notable increase in resistivity in the samples as a function of the concentration of either Co or Ni. In addition, the results of ρ vs. T with $T>T_t$ (T_t denotes the metal-insulator transition temperature) can be explained accurately at lower doping levels ($x \leq 0.1$) by means of mechanisms related to adiabatic and non-adiabatic polaron hopping. Nevertheless, increasing the concentration of either Co or Ni, the hopping mechanism of variable range can also explain the experimental results obtained here at certain temperatures more accurately. At high doping levels ($x \geq 0.5$), the experimental results describe an overall range of temperatures that fit properly into a mechanism explained as hopping at variable range.

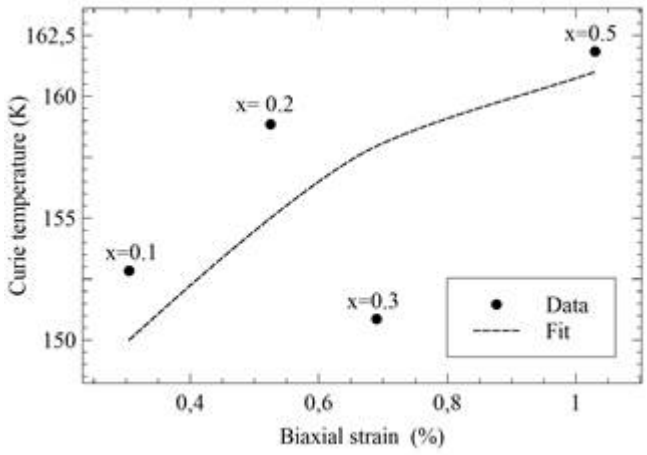

Figure 14
Evaluated biaxial strain versus Curie temperature for different compositions of $LaMn_{1-x}Ni_xO_3$ samples (x = 0.0, 0.1,0.2,0.3 and 0.5). Dashed lines are visual guides.
Source: The Authors.

In the case of $LaMn0_3$ perovskite, the Mn ions fill the B-sites, which are surrounded by 0_2 octahedrons, meeting at the corners to form a tridimensional lattice, while the Lα ions fill the A-sites between these octahedrons. Electronic conduction involves the movement of charge between orbitals d in Mn and p in 0_2 ; the p - d orbital overlap is very sensitive to geometrical changes (angles and bond lengths) generated by variations of ion size at A-sites or external applied pressure.

3. Conclusions

The $\#\alpha_{0.67-\#}\#r_{\#}\#a_{0.33}\#n_3$ samples at 0.13 ≤ # ≤ were produced by a solid state reaction method and exhibited a decrease in their lattice constants when the concentration of Pr was increased. This can be attributed to the different ionic radius size of the lanthanum and praseodymium, and the increase in "tensile" strain ($\varepsilon_{bi} > 0$). The increaset in biaxial strain causes a decrease in T_c which is fitted to a quadratic function, i.e., it is possible to assume that the biaxial strain increases the Jahn-Teller splitting (JT) from e_g levels and hence increases the localization of the electrons.

In the case of samples at 0.0 ≤ # ≤ 0.5, it was found that the adiabatic and non-adiabatic polaron transport mechanism accurately describes the outcomes of resistivity as a function of temperature. Furthermore, an increase in strain also increases the resistivity in the material, which can be attributed to the changes of the lattice constant related to the small size of the cobalt ion compared to the Mn^{3+} /Mn^{4+} ion.

In addition, in such samples it was possible to identify a double peak structure in the susceptibility measurements at higher concentrations of cobalt, which is related to the strains and the initial domain wall motion. The increase of T_c and T_t , as well as the Eα of polarons would suggest the important role of the electron-lattice interaction in this doped magnetite.

n the case of a correlation between magnetic and electric properties was observed. The substitution of nickel and cobalt into the manganese sub-lattice increases the resistance of the samples and preserves the orthorhombic structure 0′. This behavior could suggest that the range of examined substitutional levels and the experimental conditions of synthesis, used for nickel and cobalt, exhibit a behavior of trivalent ion.

In addition, such samples show an increase in terms of the biaxial strains ε_{bi}, and their temperature T_c , when the concentration of nickel is higher.

References

[1] Goodenough, J.B., Wold, A., Arnott, R.J. and Menyuk, N., Relationship between crystal symmetry and magnetic properties of ionic compounds containing Mn3+., Physical Review, 124(2), pp. 373-384, 1961. DOI: 10.1103/PhysRev.124.373

[2] Toulemonde, O., Studera, F., Barnabé, A., Maignan, A., Martin, C. and Raveau, B., Charge states of transition metal in "Cr, Co and Ni" doped Ln0.5Ca0.5MnO3 CMR manganites. The European Physical Journal B, 4(2), pp. 159-167, 1998. DOI: 10.1007/s100510050364

[3] Blasse, G., Ferromagnetic interactions in non-metallic perovskites, Journal of Physics and Chemistry of Solids, 26(12), pp. 1969-1971, 1965. DOI: 10.1016/0022-3697(65)90231-3

[4] Coey, J.M.D., Viret, M. and von Molnar, S., Mixed-valence manganites, Advances in Physics, 48(2), pp. 167-293, 1999. DOI: 10.1080/000187399243455

[5] Zener, C., Interaction between the d-Shells in the transition metals. II. Ferromagnetic compounds of manganese with perovskite structure. Physical Review, 82(3), pp. 403-405, 1951. DOI: 10.1103/PhysRev.82.403

[6] Goodenough, J.B., Wold, A., Arnott, R.J. and Menyuk, N., Relationship between crystal symmetry and magnetic properties of ionic compounds containing Mn3+. Physical Review, 124(2), pp. 373-384, 1961. DOI: 10.1103/PhysRev.124.373

[7] Ghosh, K., Ogale, S.B., Ramesh, R., Greene, R.L., Venkatesan, T., Gapchup, K.M., Bathe, R. and Patil, S.I., Transition-element doping effects in La0.7Ca0.3MnO3, Physical Review B, 59(1), pp. 533-537, 1999. DOI: 10.1103/PhysRevB.59.533

[8] Ganguly, R., Gopalakrishnan, I.K. and Yakhmi, J.V., Magnetic and electrical properties of La0.67Ca0.33MnO3 as influenced by substitution of Cr. Physica B: Condensed Matter, 275(4), pp. 308-315, 2000. DOI: 10.1016/S0921-4526(99)00855-8

[9] Yuan, S.L., Li, Z.Y., Zeng, X.Y., Zhang, G.Q., Tu, F., Peng, G., Liu, J., Jiang, Y., Yang, Y.P. and Tang, C.Q., Effect of Cu doping at the Mn site on the transport and magnetic behaviors of La2/3Ca1/3MnO3. The European Physical Journal B, 20(2), pp. 177-181, 2001. DOI: 10.1007/BF01315688

[10] Rao, C.N.R., Arulraj, A., Santhosh, P.N. and Cheetham, A.K., Charge-Ordering in Manganates. Chemistry of Material, 10(10), pp. 2714-2722, 1998. DOI: 10.1021/cm980318e

[11] Raveau, B., Maignan, A., Martin, C. and Hervieu, M., Colossal magnetoresistance manganite perovskites: relations between crystal chemistry and properties, Chemistry of Material, 10(10), pp. 2641-2652, 1998. DOI: 10.1021/cm9801791

[12] Hebert, S., Martin, C., Maignan, A., Retoux, R., Hervieu, M., Nguyen, N. and Raveau, B., Induced ferromagnetism in LaMnO3 by Mn-site substitution: The major role of Mn mixed valency, Physical Review B, 65(10), pp. 104420 1-104420 7, 2002. DOI: 10.1103/PhysRevB.65.104420

[13] Takeshi, Y., Toyoji, I. and Tadashi, K., Effect of Mn valence on crystal structure of La-Mn-O perovskite oxides. Journal of Materials Research. 10(5), pp. 1079-1082, 1995. DOI: 10.1557/JMR.1995.1079

[14] Lu, Y., Klein, J., Herbstritt, F., Philipp, J.B., Marx, A. and Gross, R., Effect of strain and tetragonal lattice distortions in doped perovskite manganites. Physical Review B, 73(18), pp. 184406 1-1844067, 2006. DOI: 10.1103/PhysRevB.73.184406

[15] Hwang, H.Y., Palstra, T.T.M., Cheong S-W. and Batlogg, B., Pressure effects on the magnetoresistance in doped manganese perovskites. Physical Review B, 52(21), pp. 15046-15049, 1995. DOI: 10.1103/PhysRevB.52.15046

[16] Millis, A.J., Quantifying strain dependence in "colossal" magnetoresistance manganites. Journal of Applied Physics, 83(3), pp. 1588-1591, 1998. DOI: 10.1063/1.367310.

[17] Goodenough J.B. and Longo, J.M., Crystallographic and magnetic properties of Perovskite and Perovskite-related compounds, in: Hellwege, K.H. and Hellwege, A.M., Eds., Magnetic and other properties of

oxides and related compounds. Landolt-Bortestein, New Series, Part of SpringerMaterials, Springer-Verlag Berlin Heidelberg, 1970. DOI: 10.1007/b19968

[18] Treves, D., Eibschutlz, M. and Coppens, P., Dependence of superexchange interaction on Fe3+#O2−#Fe3+ linkage angle. Physics Letters, 18(3), pp. 216-217, 1965. DOI: 10.1016/0031-9163(65)90294-5

[19] Torrance, J.B., Lacorre, P., Nazzal, A.I., Ansaldo, E.J. and Nierdermayer, Ch., Systematic study of insulator-metal transitions in perovskites RNiO3 (R = Pr, Nd, Sm, Eu) due to closing of charge-transfer gap. Physical Review B., 45(14), pp. 8209-8212, 1992. DOI: 10.1103/PhysRevB.45.8209.

[20] Millis, A.J., Littlewood, P.B. and Shraiman, B., Double exchange alone does not explain the resistivity of La1−xSrxMnO3. Physical Review Letters, 74(25), pp. 5144-5147, 1995. DOI: 10.1103/PhysRevLett.74.5144

[21] Millis, A.J., Shraiman, B.I. and Mueller, R., Dynamic Jahn-Teller effect and colossal magnetoresistance in La1−xSrxMnO3. Physical Review Letters. 77(1), pp. 175-178, 1996. DOI: 10.1103/PhysRevLett.77.175

[22] Millis, A.J., Mueller, R. and Shraiman, B.I., Fermi-liquid-to-polaron crossover. I. General results. Physical Review B., 54(8), pp. 5389- 5404, 1996. DOI: 10.1103/PhysRevB.54.5389

[23] Emin, D. and Holstein, T., Studies of small-polaron motion IV. Adiabatic theory of the Hall effect. Annals of Physics, 53(3), pp. 439-520, 1969. DOI: 10.1016/0003-4916(69)90034-7

[24] Veera-Krishna-Meera, K., Ravindranath, V. and Ramachandra-Rao, M.S., Magneto transport studies in La0.7Ca0.3Mn1−xMxO3 (M=Co and Ga). Journal of Alloys and Compounds. 326(1-2), pp.98-100, 2001. DOI: 10.1016/S0925-8388(01)01220-8

[25] Maignan, A., Sundaresan, A., Varadaraju, U.V. and Raveau, B., Magnetization relaxation and aging in spin-glass (La,Y)1-xCaxMnO3 (x=0.25, 0.3 and 0.5) perovskite. Journal of Magnetism and Magnetic Materials, 184(1), pp. 83-88, 1988. DOI: 10.1016/S0304-8853(97)01101-3

[26] Gontchar, L.E., Nikiforov, A.E. and Popov, S.E., Interplay between orbital, charge and magnetic orderings in R1−xAxMnO3 (x=0, 0.5). Journal of Magnetism and Magnetic Materials, 223(2), pp. 175-191, 2001. DOI: 10.1016/S0304-8853(00)00597-7.

[27] Araujo-Moreira, F.M., Rajeswari, M., Goyal, A., Ghosh, K., Smolyaninova, V., Venkatesan, T., Lobb, C.J. and Greene. R.L., Magnetic homogeneity of colossal-magnetoresistance thin films determined by alternating current magnetic susceptibility. Applied Physics Letters, 73(23), pp. 3456-3458, 1998. DOI: 10.1063/1.122795.

Notes

J.A. Olarte-Torres, received a BSc. in Physics in 1994 from the Tbilisi State University, Tbilisi, Georgia, a Sp. in Software Engineering in 1997, from the Universidad Distrital Francisco José de Caldas, Bogotá, Colombia, and an MSc. and PhD in Science Physics in 1998 and 2011, from the Universidad Nacional de Colombia, Bogotá, Colombia, respectively. From 2000 to 2007, he worked as a lecturer at Universidad Pedagógica Nacional, (Bogotá, Colombia. Currently, he is a full-time associate professor at the Department of Electronics, Facultad Tecnológica, Universidad

Distrital Francisco José de Caldas, Bogotá, Colombia. His main research interests are based on experimental condensed matter physics, and his specific research topic is the science of correlated materials as high temperature superconductors and colossal magneto-resistance manganite. ORCID: 0000-0002-9173-3685

M.C. Cifuentes-Arcila, received a BSc. in Physics Education in 2000 from the Universidad Pedagógica Nacional, Bogotá, Colombia, a Sp. and MSc. in Science Physics in 2004 and 2007 from the Universidad Nacional de Colombia, Bogotá, Colombia, respectively. She was awarded a PhD in Education in 2013 from Universidad del Valle, Cali, Colombia. From 2001 to 2004 she worked as a physics educator in a public secondary school. Currently, she is a full-time associate professor at the department of Physics, in the Facultad de Ciencia y Tecnología, Universidad Pedagógica Nacional, Bogotá, Colombia. Her main research interests are in the areas of physical science, science education and teaching quality. Her specific research topic looks at how physical science relates to experimental condensed matter physics. ORCID: 0000-0003-3237-3066

H.A. Suárez-Moreno, received a B.Sc. in Physics Education in 2010 from the Universidad Pedagógica Nacional, Bogotá, Colombia. He attained an MSc. in Science Physics in 2014, from the University of Vienna, Austria. From 2015 to 2016, he was part of the International Atomic Energy Agency as an intern, supporting different activities related to nuclear science and its applications. Currently, he is full-time assistant professor at Universidad Pedagógica Nacional, leading different lectures and seminars in the department of physics. His main research interests are based on physical science and teaching quality. His specific research topic in physical science focuses on experimental condensed matter physics, specifically spectroscopy techniques for the characterization of new materials, quantum optics techniques, and low-energy electron diffraction technique. ORCID: 0000-0001-8092-9749

How to cite: Olarte-Torres, J.A, Cifuentes-Arcila, M.C. and Suárez-Moreno, H.A, Effects of strain on $L\alpha_{0.67-x}Pr_x$ $C\alpha_{0.33}Mn0_3$, $L\alpha Mn_{1-X}C0_x$ 0_3 and $L\alpha Mn_{1-x}Ni_x$ 0_3 magnetite simples. DYNA, 86(211), pp. 278-287, October - December, 2019.